

High-speed XYZ-nanopositioner for scanning ion conductance microscopy

Shinji Watanabe^{1, a)} and Toshio Ando^{1, b)}

Bio-AFM Frontier Research Center, Institute of Science and Engineering, Kanazawa University, Kakuma-machi, Kanazawa 920-1192, Japan

We describe a tip-scan-type high-speed XYZ-nanopositioner designed for scanning ion conductance microscopy (SICM). The nanopipette probe is mounted in the center of a hollow piezoactuator, both ends of which are attached to identical diaphragm flexures, for Z-positioning. This design minimizes the generation of undesirable mechanical vibrations. Mechanical amplification is used to increase the XY-travel range of the nanopositioner. The first resonance frequencies of the nanopositioner are measured as ~ 100 and ~ 2.3 kHz for the Z- and XY-displacements, respectively. The travel ranges are ~ 6 and ~ 34 μm for Z and XY, respectively. When this nanopositioner is used for hopping mode imaging of SICM with a ~ 20 -nm diameter tip, the vertical tip velocity can be increased to 400 nm/ms; hence, the one-pixel acquisition time can be minimized to ~ 1 ms.

In biological research, atomic force microscopy (AFM)¹ has been widely used to visualize the topographic structure of biological specimens under physiological liquid environments². Nevertheless, the cantilever tip must make contact with the sample in the solution, and even exerted forces below 10 pN considerably deform extremely soft surfaces^{3,4} such as the plasma membranes of live eukaryotic cells, which prohibits high-resolution surface imaging⁵. Scanning ion conductance microscopy (SICM) is an alternative imaging method based on an entirely different working principle for capturing a topographic image⁶ (Fig. 1). SICM uses an electrolyte-filled glass pipette (nanopipette) as a probe and relies on an ion current flowing between an electrode inside the nanopipette and another in an external bath solution. The ion current passing through the opening of the nanopipette is sensitive to the tip-sample surface separation^{7,8}; therefore, SICM can capture topographic images without any tip-sample contact.

However, the temporal resolution of SICM is much lower than that of AFM, especially when SICM is operated in the hopping mode⁹, where the tip is moved up and down to avoid lateral tip-sample contact. This low temporal resolution, due to the time delay in the vertical tip-position control, limits the fall velocity of the tip, v_f ; namely, the speed at which the tip approaches the sample surface. Since glass nanopipettes are very fragile, they are easily damaged when they contact surfaces. To avoid surface contact, v_f must be restricted. When the bandwidth of the ion current detection is sufficiently high, the low mechanical resonance frequency of the Z-nanopositioner is the dominant contributor to the delay¹⁰. The difficulty to decrease the delay is how to assemble the nanopipette to the Z-nanopositioner since the nanopipette is very massive and large compared to AFM cantilever tip. For instance, commercial SICM systems use a long-travel-range (~ 25 μm) Z-nanopositioner whose resonance frequency is less than 1 kHz when the

nanopipette is assembled, producing a long delay (longer than 1 ms) for vertical tip positioning. As a result, it typically takes 10–100 ms for one-pixel acquisition when imaging samples showing very rough surfaces⁹. Thus, in SICM, it is difficult to visualize morphological changes in samples that occur in under a minute, which significantly limits the applicability of SICM in biological studies.

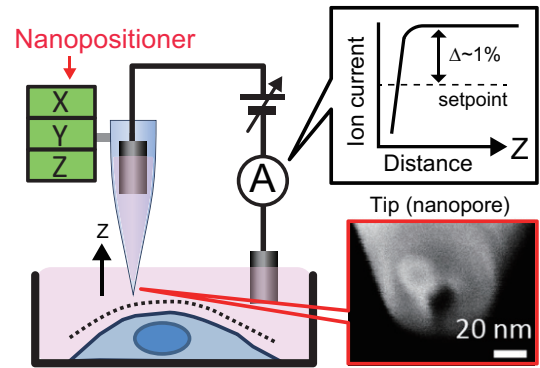


FIG. 1. (Color online) Schematic of typical SICM setup showing working principle of SICM. The electrolyte-filled nanopipette mounted on the XYZ-nanopositioner has a nanopore at its distal end, as shown in the electron micrograph (right bottom). The ion current flowing through the nanopore induced by the application of bias voltage between two electrodes (one in the nanopipette, the other in the bath solution) is measured using the ion current detector. The ion current, which depends on the tip-surface separation as illustrated (right top), is used to control the tip Z-position during the XY-scanning of the nanopipette over the sample surface.

In this letter, we describe the design of a tip-scan-type high-speed XYZ-nanopositioner for SICM. One of the distinctive features of the developed nanopositioner is the large product of “travel range \times resonance frequency” for the Z-positioner, which represents the positioner performance because the travel range and resonance frequency are tradeoffs. The product of our Z-positioner, $6 \mu\text{m} \times 100 \text{ kHz}$, is more than ten-fold larger than those of conventional SICM systems and 2–3 times larger than that of the Z-scanner employed in high-speed AFM¹¹. The performance can significantly

^{a)} wshinji@se.kanazawa-u.ac.jp;

^{b)} tando@staff.kanazawa-u.ac.jp;

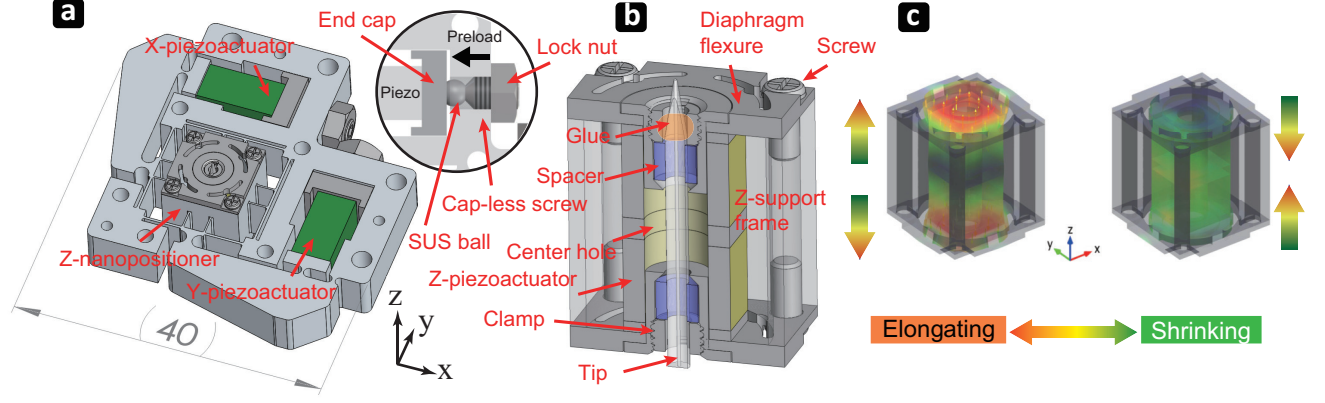


FIG. 2. (Color online) (a) Drawing showing structure of XYZ-nanopositioner designed in this study. The base frame is 5 mm thick and 40 mm wide. The lateral scan is driven with identical piezoactuators via mechanical amplification. Preloads are applied to the X- and Y-piezoactuators using the end caps, each of which is pushed with the capless screw via a stainless steel ball. To stabilize the preload, each screw is fixed with a lock nut. (b) Cross-sectional view of the Z-nanopositioner. The glue is only applied to a contact area between the top clamp and the nanopipette. (c) Displacement of Z-nanopositioner in the elongation (left) and shrinkage (right) actuations, as simulated by FEA. The arrows represent the vectors of local displacement from its original position.

increase v_f to 400–600 nm/ms and hence minimize the one-pixel acquisition time to ~ 1 ms. Here, we show the detailed design and performance of our nanopositioner and demonstrate the stable high-speed imaging of test samples at 3.5 s per frame over a scan area of $\sim 25 \times 25 \mu\text{m}^2$ with 50×50 pixels.

The Z-nanopositioner mounted on the XY-nanopositioner, as illustrated in Fig. 2(a), is designed to achieve a high mechanical resonance frequency and hence a large v_f . The frame body of the XYZ-nanopositioner was fabricated from alloy A7075. Before constructing the actual device, we conducted a finite-element analysis (FEA) to estimate the mechanical properties of designed structures, using a commercially available finite-element package, COMSOL Multiphysics 5.0 (COMSOL AB). The following mechanical parameters for the alloy A7075/piezoactuator were used in the FEA simulation: Young's modulus, 72/33.9 GPa; Poisson's ratio, 0.3/0.3; density, 2810/7800 kg/m³. The central idea for suppressing unwanted mechanical vibrations in the Z-nanopositioner is the use of momentum cancellation¹². That is, the hollow Z-piezoactuator (AE0505D08D-H0F, NEC/Tokin) is sandwiched with a pair of identical diaphragm-like flexures¹³ [Fig. 2(b)] so that the center of mass of the Z-piezoactuator shows negligible change during fast displacement. The flexures were designed to have a stiffness of ~ 18.2 N/ μm , which provides a suitable preload to the actuator (~ 10 –20 N). The magnitude of the preload is adjustable with screws.

This design can mechanically cancel dynamic forces exerted onto the Z-support frame when the Z-piezoactuator is quickly displaced. Moreover, it permits the Z-positioner to have a resonance frequency comparable to that of the Z-piezoactuator under free oscillation.

Injecting epoxy glue between the diaphragm flexures and the Z-piezoactuator improved the mechanical stability of the Z-positioner and enabled its robust long-term actuation. The ~ 12 –14-mm-long nanopipette is mechanically connected to the top flexure by gluing the nanopipette only to the top clamp [Fig. 2(b)] so that the nanopipette can move with the z-movement of the top flexure. In order to avoid unintentional mechanical vibrations of the nanopipette, the nanopipette length was shortened as much as possible and the nanopipette was supported by the spacers made of an elastic material at the top and bottom clamps. A polyimide tube inserted between the nanopipette at the glue point enhances the fixing strength between the nanopipette to the clamp. This assembly only decreases the resonance frequency of the Z-piezoactuator by 10% since the total mass of the nanopipette and clamp are much smaller than that of the Z-piezoactuator. Importantly, undesirable vibrations were suppressed in the Z-positioner below the first resonance frequency at 100 kHz [Fig. 3(a)]. The measured first resonance frequency agreed reasonably well with the result of the FEA simulation [Fig. 3(b)]. The travel range of Z-nanopositioner was $\sim 6 \mu\text{m}$, as measured with a laser vibrometer (NLV-2500, Polytech), approximately half the original maximum displacement of the Z-piezoactuator, as expected. Since the travel range is inversely proportional to the resonance frequency¹⁴, the performance of our Z-nanopositioner can be evaluated from the product of travel range \times resonance frequency, which at $6 \mu\text{m} \times 100$ kHz significantly exceeds (by more than 10-fold) the $25 \mu\text{m} \times 1$ –2 kHz shown in conventional SICM nanopositioners.

For XY-displacements, we used mechanical amplification¹⁵ to magnify the original travel range (9 μm at 150 V) of XY-piezoactuators (AE0505D08DF, NEC/Tokin).

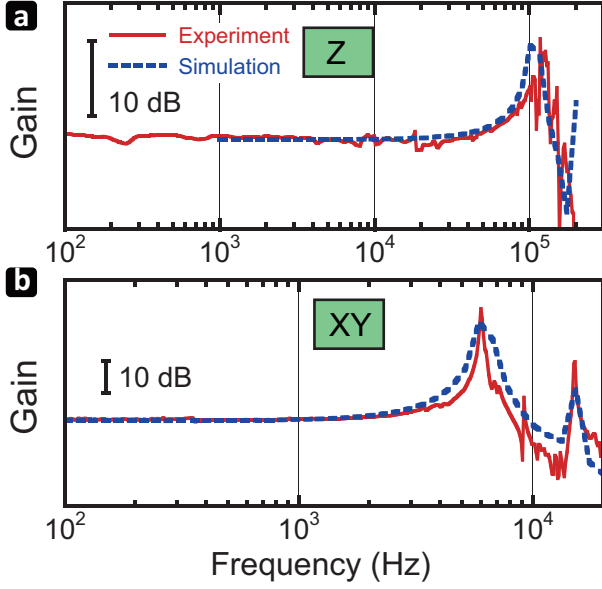


FIG. 3. (Color online) Transfer function of nanopositioner for (a) vertical and (b) lateral displacements (phase is not shown). The solid and broken lines indicate the results from experiments and FEA simulations, respectively. The transfer functions were obtained for the 300- μm -thick beam flexures. The resonance frequency for the lateral displacement decreases from ~ 6 to 4.5 kHz when the full components of Z-positioner are assembled with the XY-positioner.

In our XY-nanopositioner design, the XY-travel range can be controlled by varying the thickness of the beam flexures that connect the Z-nanopositioner and the surrounding base frame, indicated by the broken circle in [Fig. 4(c)], without changing the overall dimensions of the nanopositioner. The measured travel range increased from 16 [Fig. 4(a)] to 34 μm [Fig. 4(b)] with decreasing beam-flexure thickness from 300 to 200 μm , which is the practical limit for fabrication by wire electrical discharge machining. The mechanical amplification factors, 1.4 and 2.7, were consistent with the results of the FEA simulation (not shown). The measured dominant resonance frequency of the XY-nanopositioner assembled with the full components of the Z-nanopositioner decreased from 4.5 to 2.3 kHz, adequate for achieving high-speed SICM, with decreasing beam-flexure thickness (not shown).

We first captured hopping-mode SICM images of Grating 1 samples immersed in a solution containing 0.15 M KCl. The v_f and hopping amplitude were set at 400 nm/ms and 300 nm, respectively. Figure 5(a) shows a topographic image captured at 3.5 s/frame for a scan range of $\sim 25 \times 25 \mu\text{m}^2$ with 50×50 pixels. The image shows a grating pitch with variations of 20% in the X- and Y-directions, mainly due to the hysteresis effect of the XY-piezoactuators and partially due to the cross-coupling between them. Since it is possible to compensate for these effects by exploiting previously reported methods^{10,16}, we do not focus on this issue

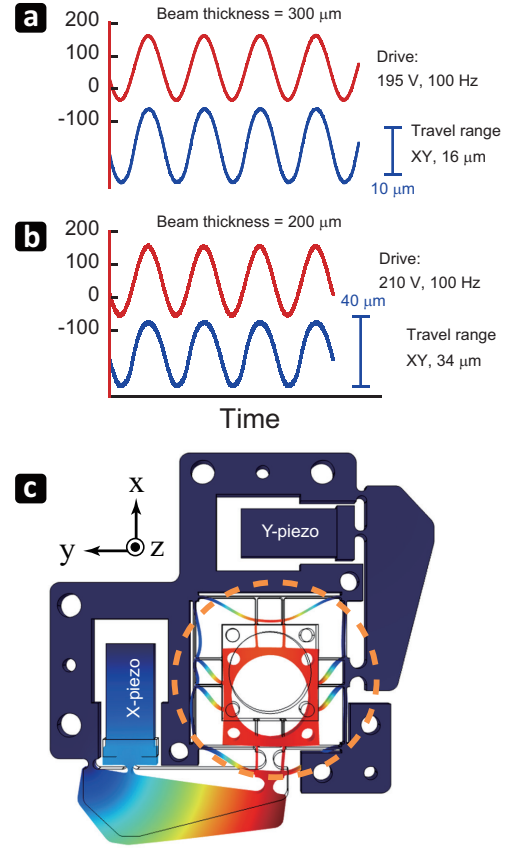


FIG. 4. (Color online) Lateral displacements of the nanopositioner under 100-Hz sinusoidal voltage application. The beam flexures are (a) 300 and (b) 200 μm thick. (c) FEA simulation result for the elongation of the X-piezoactuator. In this simulation, the positions of the backside of the piezoactuator and the screw holes in the scanner frame were fixed.

in this study. In Fig. 5(a), no notable undesirable vibrations appeared even at the left edge region of the image, where the scanning direction was inverted and hence the X-positioner was driven at high frequencies. The v_f value, 400 nm/ms, used in this imaging is significantly larger than the typical v_f values used in conventional SICM systems (~ 20 nm/ms). Although the comparable v_f value ~ 500 nm/ms was reported for a large nanopore diameter ~ 100 nm⁸, attainable v_f value will decrease to ~ 100 nm/ms when the previous report uses an identical nanopore diameter (~ 20 nm) used in this study. Therefore, our positioner significantly improved the v_f .

We first captured hopping-mode SICM images of Grating 1 samples immersed in a solution containing 0.15 M KCl. The v_f and hopping amplitude were set at 400 nm/ms and 300 nm, respectively. Figure 5(a) shows a topographic image captured at 3.5 s/frame for a scan range of $\sim 25 \times 25 \mu\text{m}^2$ with 50×50 pixels. The image shows a grating pitch with variations of 20% in the X- and Y-directions, mainly due to the hysteresis

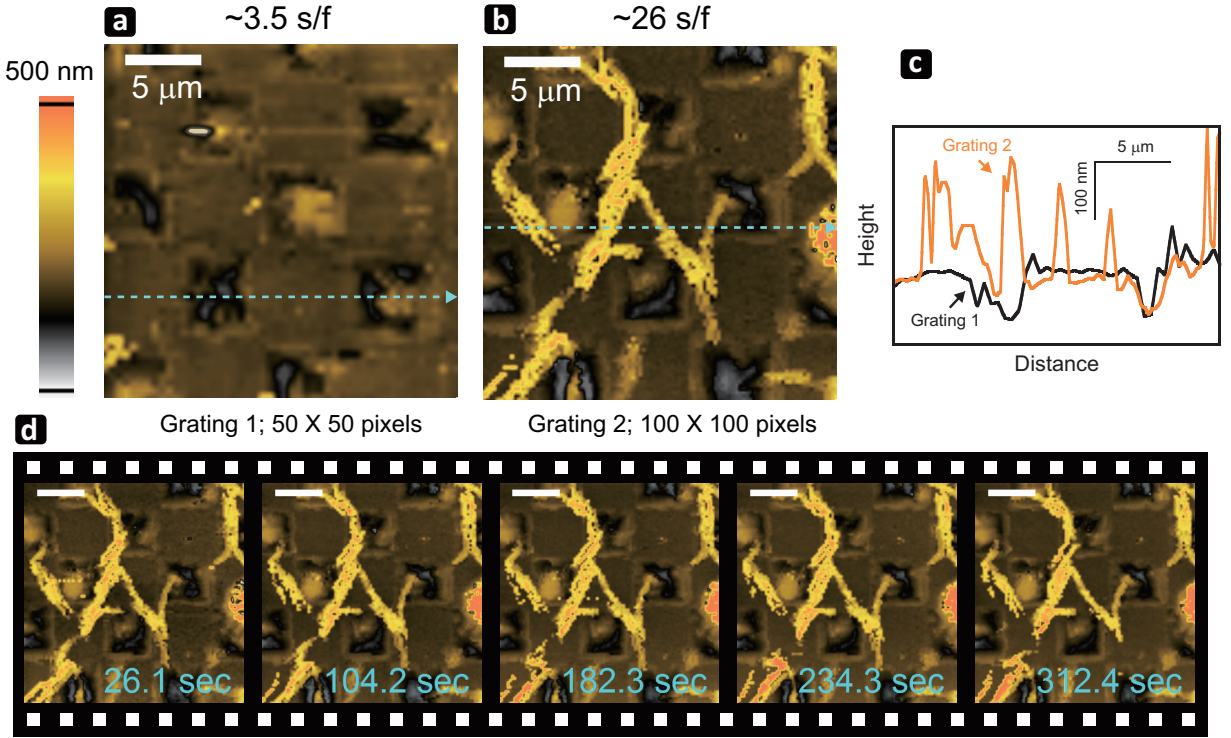


FIG. 5. (Color online) SICM images of Gratings (a) 1 and (b) 2 captured at 3.5 and 26 s/frame, respectively. (c) Height profiles of images (a) and (b) along the light blue broken lines shown in (a) and (b). (d) Five images of Grating 2 clipped from successive images captured at ~26 s/frame for longer than 5 min. Scale bars, 5 μm .

effect of the XY-piezoactuators and partially due to the cross-coupling between them. Since it is possible to compensate for these effects by exploiting previously reported methods^{10,16}, we do not focus on this issue in this study. In Fig. 5(a), no notable undesirable vibrations appeared even at the left edge region of the image, where the scanning direction was inverted and hence the X-positioner was driven at high frequencies. The v_f value, 400 nm/ms, used in this imaging is significantly larger than the typical v_f values used in conventional SICM systems (~ 20 nm/ms). Although the comparable v_f value ~ 500 nm/ms was reported for a large nanopore diameter ~ 100 nm⁸, attainable v_f value will decrease to ~ 100 nm/ms when the previous report uses an identical nanopore diameter (~ 20 nm) used in this study. Therefore, our positioner significantly improved the v_f .

To further evaluate the performance of our XYZ-nanopositioner, we captured a topographic image of Grating 2 with rougher surfaces than Grating 1, in which wire-like objects were seen on the surface, as shown in Fig. 5(b). This image was captured at ~ 26 s/frame for a scan range of $\sim 25 \times 25 \mu\text{m}^2$ with 100×100 pixels, using a hopping amplitude of 600 nm and v_f of 400 nm/ms. By increasing the hopping amplitude to 600 nm, wire-like objects likely to be partially suspended between grids [Fig. 5(c)] were captured without their disruption, although the time required for one-pixel

acquisition increased from ~ 750 to $1500 \mu\text{s}$. Figure 5(d) shows successive images of Grating 2 captured for longer than 5 min. Since touching the surface manifests as ‘tail like patterns’ in observed images regardless with the stiffness of wire-like objects¹⁷, no noticeable changes in these images demonstrate the robustness of our XYZ-positioning.

In summary, we developed a tip-scan-type high-speed XYZ-nanopositioner for SICM. The installation of the nanopipette mount in the center of a hollow piezoactuator and the use of a momentum cancellation mechanism for the Z-positioner resulted in a high resonance frequency of 100 kHz even with a relatively long travel range, 6 μm . The improved time delay of the Z-nanopositioner increases the v_f by more than 20 times that of conventional SICM nanopositioners. These excellent features allowed the high-speed imaging of Grating 1 at 3.5 s/frame for a scan area of $25 \times 25 \mu\text{m}^2$ with 50×50 pixels without generating undesirable vibrations. Moreover, a rougher surface could be captured without decreasing v_f . This study is the first step toward achieving high-speed SICM that can capture biological samples in dynamic action in real time.

This work was supported by the grant for ‘JST-SENTAN’ (to S.W.) and the Grant for Young Scientists from Hokuriku Bank (to S.W.) and JSPS KAKENHI; Grant Numbers JP26790048 (to S.W.), JP16H00799 (to S.W.), and JP26119003 (to T.A.).

- ¹G. Binnig, C. F. Quate, and C. Gerber, "Atomic force microscope," *Physical review letters* **56**, 930 (1986).
- ²Y. F. Dufrène, T. Ando, R. Garcia, D. Alsteens, D. Martinez-Martin, A. Engel, C. Gerber, and D. J. Müller, "Imaging modes of atomic force microscopy for application in molecular and cell biology," *Nature Nanotechnology* **12**, 295–307 (2017).
- ³Y. Zhou, C.-C. Chen, A. E. Weber, L. Zhou, L. A. Baker, and J. Hou, "Potentiometric-scanning ion conductance microscopy for measurement at tight junctions," *Tissue barriers* **1**, e25585 (2013).
- ⁴T. Ushiki, M. Nakajima, M. Choi, S.-J. Cho, and F. Iwata, "Scanning ion conductance microscopy for imaging biological samples in liquid: A comparative study with atomic force microscopy and scanning electron microscopy," *Micron* **43**, 1390–1398 (2012).
- ⁵J. Seifert, J. Rheinlaender, P. Novak, Y. E. Korchev, and T. E. Schäffer, "Comparison of atomic force microscopy and scanning ion conductance microscopy for live cell imaging," *Langmuir* **31**, 6807–6813 (2015).
- ⁶P. Hansma, B. Drake, O. Marti, S. Gould, and C. Prater, "The scanning ion-conductance microscope," *Science* **243**, 641–643 (1989).
- ⁷Y. E. Korchev, C. L. Bashford, M. Milovanovic, I. Vodyanoy, and M. J. Lab, "Scanning ion conductance microscopy of living cells," *Biophysical journal* **73**, 653–658 (1997).
- ⁸P. Novak, A. Shevchuk, P. Ruenaroengsak, M. Miragoli, A. J. Thorley, D. Klenerman, M. J. Lab, T. D. Tetley, J. Gorelik, and Y. E. Korchev, "Imaging single nanoparticle interactions with human lung cells using fast ion conductance microscopy," *Nano letters* **14**, 1202–1207 (2014).
- ⁹P. Novak, C. Li, A. I. Shevchuk, R. Stepanyan, M. Caldwell, S. Hughes, T. G. Smart, J. Gorelik, V. P. Ostanin, M. J. Lab, G. W. J. Moss, G. I. Frolenkov, D. Klenerman, and Y. E. Korchev, "Nanoscale live-cell imaging using hopping probe ion conductance microscopy," *Nature methods* **6**, 279–281 (2009).
- ¹⁰Y. K. Yong, K. Liu, and S. R. Moheimani, "Reducing cross-coupling in a compliant xy nanopositioner for fast and accurate raster scanning," *IEEE Transactions on Control Systems Technology* **18**, 1172–1179 (2010).
- ¹¹T. Ando, T. Uchihashi, and T. Fukuma, "High-speed atomic force microscopy for nano-visualization of dynamic biomolecular processes," *Progress in Surface Science* **83**, 337–437 (2008).
- ¹²T. Ando, N. Kodera, E. Takai, D. Maruyama, K. Saito, and A. Toda, "A high-speed atomic force microscope for studying biological macromolecules," *Proceedings of the National Academy of Sciences* **98**, 12468–12472 (2001).
- ¹³Y. Yong and S. R. Moheimani, "Design of an inertially counterbalanced z-nanopositioner for high-speed atomic force microscopy," *IEEE Transactions on Nanotechnology* **12**, 137–145 (2012).
- ¹⁴Y. K. Yong, S. O. R. Moheimani, B. J. Kenton, and K. K. Leang, "Invited review article: High-speed flexure-guided nanopositioning: Mechanical design and control issues," *Review of Scientific Instruments* **83**, 121101 (2012).
- ¹⁵Y. K. Yong, S. S. Aphale, and S. R. Moheimani, "Design, identification, and control of a flexure-based xy stage for fast nanoscale positioning," *IEEE Transactions on Nanotechnology* **8**, 46–54 (2009).
- ¹⁶H. Watanabe, T. Uchihashi, T. Kobashi, M. Shibata, J. Nishiyama, R. Yasuda, and T. Ando, "Wide-area scanner for high-speed atomic force microscopy," *Review of Scientific Instruments* **84**, 053702 (2013).
- ¹⁷D. Klenerman, Y. E. Korchev, and S. J. Davis, "Imaging and characterisation of the surface of live cells," *Current opinion in chemical biology* **15**, 696–703 (2011).